# Vehicle Trajectory Estimation Using a High-Gain Multi-Output Nonlinear Observer\*

Hamidreza Alai, Ali Zemouche, and Rajesh Rajamani

Abstract— This paper focuses on the design of a multi-output high gain observer for a vehicle trajectory tracking application. Tracking the trajectories of other vehicles on the road is needed for many applications ranging from collision avoidance to autonomous driving. Previously, such trajectory tracking has been done using linearized dynamic models, interactingmultiple-model (IMM) filters, or else by using LMI-based nonlinear observers. These estimation techniques suffer from some crucial shortcomings. Hence, this paper develops a high gain nonlinear observer for this application. The high gain observer approach offers the advantages of guaranteed feasibility and stability with just one constant observer gain for a wide range of motion. The challenges of transforming the vehicle dynamic model into the required companion form for applying the high gain observer technique are addressed. A coordinate transformation that allows for varying velocity and varying slip angle is shown to be appropriate. The high gain observer methodology for a dynamic system with multiple outputs is presented. Finally, simulation and experimental results on vehicle tracking are demonstrated. The experimental results show that, with a high gain observer, vehicle trajectories that span a large range of orientations can be accurately tracked using just one constant observer gain.

Key words – vehicle trajectory estimation; vehicle control; filters; estimation algorithms; nonlinear observer; e-scooter.

#### I. INTRODUCTION

#### A. Vehicle Tracking Problem

While estimation and control of the ego vehicle's variables are crucial elements in autonomous driving [1], tracking surrounding vehicles is also a critical aspect for collision avoidance [2]. By tracking the trajectories of other vehicles on the road, essential variables in collision prediction (e. g. time-to-collision) can be calculated using estimates of the vehicles' position, velocity, and orientation [3]. Hence, designing observers to accurately estimate surrounding vehicles' states is valuable [4, 5]. However, vehicle motion typically involves nonlinear dynamic models. Some of the previous works addressed this problem by turning the original nonlinear model into multiple linear models typically including a "straight line driving" and a "constant turn rate driving" model [6, 7]. Using these linear models, they utilize Interacting Multiple Model (IMM) filters (e. g. IMM Kalman Filters) for state estimation [6, 7]. These papers based on linearization lack a proof of stability and do not cover all possible maneuvers. Also, implementing IMM filters is more

computationally demanding as they require real-time evaluation of each model's probability.

Several authors have recently explored new types of filters and estimators for vehicle tracking. For example, Kim, et.al., proposed a vehicle tracking algorithm based on a L-shaped vehicle model with switching for use with a laser scanner [8]. Jo, et. al. presented a unified vehicle tracking and behavior reasoning algorithm that simultaneously estimated the vehicle dynamic state and driver intentions based on a multiple model filter [9]. Cao, et. al. proposed a radar-based tracking method in which the vehicle's rectangular area is partitioned into multiple regions and an approach is proposed to associate measurements with these regions [10]. All these methods relied on stochastic estimators or "filters". Stochastic estimators such as the Kalman filter and the extended Kalman filter rely on linearization of the nonlinear vehicle motion model [9, 10]. When the inherent dynamic system model is nonlinear, the global stability of the estimator is not guaranteed [11, 12]. Compared to the extended Kalman filter, the nonlinear high-gain observer comes with guaranteed global stability for the entire operating range of the system.

In the domain of deterministic model-based estimators or "observers", a few papers have investigated the use of LMIbased nonlinear observers for vehicle state estimation [2, 13]. Such nonlinear observers are obtained based on a single nonlinear model and include constant observer gains. Thus, they are easy to implement. However, they have some shortcomings including limited stability regions and simplifying assumptions in the model (e.g., assumption of constant velocity). The designed observers are guaranteed to be stable only for a small region of steering angle and limited range of vehicle direction angle due to the non-monotonic nonlinear functions involved in the model. Therefore, switched gain observers with different gains in different piecewise regions were required to cover the entire operating range. Also, these observers assume constant velocity and are not able to accurately estimate the states of vehicles with variable velocities. Hence, this paper will design high-gain observers allowing for variable velocity, guaranteed stability, and guaranteed feasibility.

## B. Challenges of High-Gain Observer Design

LMI (Linear Matrix Inequality) based nonlinear observers [13, 14] are powerful tools in state estimation as they have proof of stability and are relatively easy to implement in real-

<sup>\*</sup> Research supported in part by a research grant from the National Science Foundation (NSF Grant CPS 2038403). The work of Ali Zemouche was supported by the ANR project ArtISMo ANR-20-CE48-0015.

R. Rajamani and H. Alai are with the Department of Mechanical Engineering, University of Minnesota, Twin Cities, Minneapolis, MN 55455 USA (Email: rajamani@umn.edu; TEL: 612-626-7961; alai0003@umn.edu)

A. Zemouche is with the University of Lorraine, CRAN UMR 7039, 54400 Cosnes et Romain, France (Email: ali.zemouche@univlorraine.fr).

world cases. The observer gain needs to be found by solving a LMI problem. If found, the LMI is feasible and the observer dynamics will be stable. However, there is no guarantee that a solution can be found for a specific application. Therefore, one of the challenges of designing these observers is the unknown feasibility of the LMI problem: the existence of stable observer gains is not guaranteed.

A different kind of estimator is the high-gain observer [15]. For nonlinear systems in (transpose) companion form, stable high-gain observers are guaranteed to exist, if the involved nonlinear functions are Lipschitz [15, 16, 17]. Thus, the highgain observer always has a feasible solution, while the LMIbased observers in general do not. With all the benefits of using high-gain observers, very few real-world applications of these observers can be found in the literature as the transformation of the nonlinear systems into the required companion form is non-trivial. Also, multi-output applications of high-gain observers have been seldom (if at all) utilized in the literature. In this paper, we show how to design a high gain observer for a vehicle system that is originally not in the companion form and has multiple outputs. The design process can be inspiring for other systems and might help lead to more practical applications of highgain observers in the future.

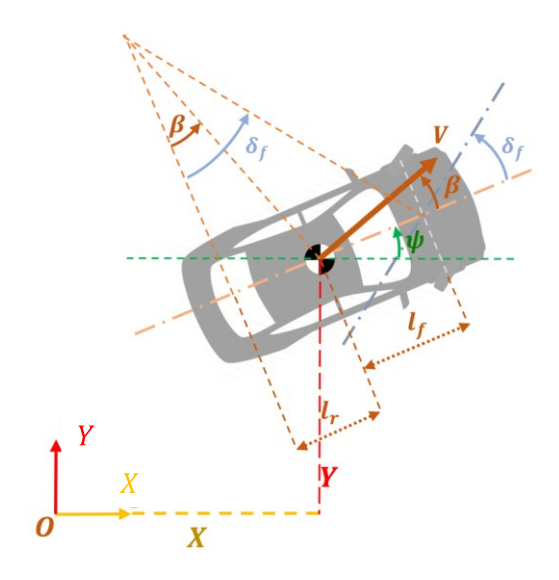
The primary contributions of the paper are as follows:

- The paper presents the challenges in transforming the vehicle tracking system model to the companion form needed for high gain observer design. Both failure and success in achieving this transformation are discussed.
- This paper is possibly one of the first ever utilizations of a multi-output high gain observer to a real-world application.
- 3) The paper demonstrates a successful solution to the vehicle tracking application with significant advantages compared to previous attempts in literature:
  - Unlike interacting-multiple-model filters which utilize multiple linearized models, the developed high gain observer provides guaranteed stability, does not use linearization and is computationally more efficient.
  - b) Unlike LMI-based observers which do not have guaranteed feasibility and require switched gains, the high gain observer works with a single constant gain over a wide range of operating conditions and has guaranteed feasibility.

The outline of the paper is as follows. In section II, it is shown how to transform the original vehicle model into the companion form. Section III describes the design of a highgain observer for the multi-output vehicle model. Section IV shows how the high-gain observer outperforms previous nonlinear observers for vehicle tracking in simulation. Experimental results for the high-gain observer are presented in section V. Section VI contains the conclusions.

#### II. VEHICLE MODEL TRANSFORMATION

In this section, we investigate the transformation of a vehicle model to the companion form needed for the high-gain observer design. For each measured output of the system  $(y_i)$ , the companion form needs the system to have a specific relationship between the states of the following form:



 $y_i = x_m, \dot{x}_m = x_{m+1}, \dots, \dot{x}_{m+r-1} = x_{m+r}, \quad \dot{x}_{m+r} = f(x)$ Since most systems are not in the companion form to start with one has to find a coordinate transformation to bring the

with, one has to find a coordinate transformation to bring the system into this form. A standard transformation of the original vehicle model comes with significant disadvantages. A modified model, on the other hand, is much more effective for transformation into the companion form.

## A. Original Vehicle Model

Fig. 2 shows a vehicle with velocity V, orientation (yaw) angle  $\psi$ , slip angle  $\beta$ , and steering angle  $\delta_f$ . In this paper, it is assumed that the steering angle changes slowly, i.e., its derivative is small. Such an assumption will hold for nominal lane change and slow turning maneuvers. The original vehicle (bicycle) model considered in this paper is [3]:

$$\dot{X} = V\cos(\psi + \beta) \tag{1}$$

$$\dot{Y} = V \sin(\psi + \beta) \tag{2}$$

$$\dot{\psi} = V(\cos\beta) \tan \delta_f / l \tag{3}$$

$$\dot{\delta}_f = 0 \tag{4}$$

where the parameter l is the wheelbase length of the vehicle:

$$l = l_f + l_r \tag{5}$$

Parameters  $l_f$  and  $l_r$  are shown in Fig. 1. Also, we use the following relationship between the slip and steering angles [3]:

$$\beta = \tan^{-1} \left( \frac{\ell_r \tan(\delta_f)}{\ell_f + \ell_r} \right) \tag{6}$$

In this paper, the slip angle of the vehicle  $\beta$  is assumed to change slowly and hence its rate of change is assumed to be negligible or zero. Note that by rewriting (6) as:

$$\frac{\tan \beta}{l_r} = \frac{\tan(\delta_f)}{l} \tag{7}$$

and substituting in (3), we get:

$$\dot{\psi} = V \sin \beta / l_r \tag{8}$$

#### B. Transformation of the Vehicle Model

We start with the following states and output vectors:

$$x = [X \quad Y \quad \psi \quad \delta_f]^T, y = [X \quad Y]^T \tag{9}$$

Speed  $(V_1)$  is not included in the state vector (9) but is obtained approximately from numerical differentiation of the measurements. The assumptions in the simplified model are:

$$\dot{V} = 0, \qquad V = V_1, \qquad \dot{\beta} = 0 \tag{10}$$

leading to the following vehicle model (based on (1)- (10)):

$$\dot{x} = \begin{bmatrix} \dot{X} \\ \dot{Y} \\ \dot{\psi} \\ \dot{\beta} \end{bmatrix} = \begin{bmatrix} V_1 \cos(\psi) \\ V_1 \sin(\psi) \\ V_1 \sin \beta / l_r \\ 0 \end{bmatrix}$$
(11)

The companion form requires using the two outputs and their derivatives as the states. To transform the model into companion form, define:

$$w_1 = y_1 = X$$
,  $w_2 = y_2 = Y$  (12)

Find the derivative of (12) and use (1) and (2):

$$\dot{w}_1 = w_3 = \dot{X} = V_1 \cos(\psi) \tag{13}$$

$$\dot{w}_2 = w_4 = \dot{Y} = V_1 \sin(\psi) \tag{14}$$

The dynamic of  $\dot{\psi}$  is not captured yet and another derivative is required. Use (11), (13), and (14) to obtain:

$$\ddot{w}_1 = \dot{w}_3 = w_5 = \ddot{X} = -V_1^2 \sin \beta \sin(\psi) / l_r \qquad (15)$$

$$\ddot{w}_2 = \dot{w}_4 = w_6 = \ddot{Y} = V_1^2 \sin \beta \cos(\psi) / l_r \qquad (16)$$

Note that  $\ddot{w}_1$  and  $\ddot{w}_2$  cannot be written in terms of  $w_1$ ,  $w_2$ ,  $w_3$ , and  $w_4$ . Therefore, based on (10), (11), (15), and (16):

$$\ddot{w}_1 = \dot{w}_5 = \ddot{X} = -V_1^3 \sin^2 \beta \cos(\psi) / l_r^2 \tag{17}$$

$$\ddot{w}_2 = \dot{w}_6 = \ddot{Y} = -V_1^3 \sin^2 \beta \sin(\psi) / l_r^2$$
 (18)

Considering (15)- (18),  $\frac{V_1 \sin \beta}{l_r}$  is related to the new states:

$$(w_6w_3 - w_5w_4)/V_1^2 = V_1\sin\beta/l_r \tag{19}$$

Replacing (19), (13), and (14) in (17) and (18):

$$\dot{w}_5 = -w_3 \left( \frac{w_6 w_3 - w_5 w_4}{V_1^2} \right)^2 \tag{20}$$

$$\dot{w}_6 = -w_4 \left( \frac{w_6 w_3 - w_5 w_4}{V_1^2} \right)^2 \tag{21}$$

In summary, the transformed model in companion form is:

and

$$f(w) = \begin{bmatrix} \dot{w}_5 \\ \dot{w}_6 \end{bmatrix} = \begin{bmatrix} -w_3 \left( \frac{w_6 w_3 - w_5 w_4}{V_1^2} \right)^2 \\ -w_4 \left( \frac{w_6 w_3 - w_5 w_4}{V_1^2} \right)^2 \end{bmatrix}$$
(23)

While the model (11) had four states, the transformed

system (22) has six states. The redundancy of model (22) can be explained by two constraints. The first constraint is  $V = V_1$  from (10). Note that we have  $w_3 = \dot{X}$  and  $w_4 = \dot{Y}$  from (13) and (14). The first constraint can be written as:

$$w_3^2 + w_4^2 = V_1^2 (24)$$

The second constraint comes from the constant velocity or  $\dot{V} = A \approx 0$  based on (10). Note that from (15) and (16) we have  $\dot{w}_3 = w_5$  and  $\dot{w}_4 = w_6$ . Therefore, taking derivative from (24) will give us the second constraint:

$$w_3 w_5 + w_4 w_6 = 0 (25)$$

A fourth order system has been translated to a sixth order system plus two constraints. To design a high-gain observer only model (20) must be utilized. The constraints (24) and (25) must be ignored and cannot be utilized in the estimation, since the high gain observer cannot utilize a model involving constraint equations.

## C. Transformation of a Modified Vehicle Model

By removing some of the assumptions in (10), we improved the previous model and solved the issue with the disadvantages of increase in system order:

- Instead of constant velocity, we assume constant acceleration so that the observer will have much better performance when the velocity is changing.
- ii) Also, the assumption that the velocity  $V = V_1$  is known is no longer needed.

The states and output vectors for the improved model are:

$$x = [X \quad Y \quad V \quad A \quad \psi \quad \beta]^T, y = [X \quad Y]^T \quad (26)$$

Thus, two new states V and A have been added. The new assumption is:

$$\dot{A} \approx 0$$
 (27)

Also, from (4) and (6):

$$\dot{\beta} \approx 0 \tag{28}$$

The improved vehicle model based on assumptions (27) is:

$$\dot{x} = \begin{bmatrix} \dot{X} \\ \dot{Y} \\ \dot{Y} \\ \dot{Q} \\ \dot{\psi} \\ \dot{\beta} \end{bmatrix} = \begin{bmatrix} V\cos(\psi + \beta) \\ V\sin(\psi + \beta) \\ A \\ 0 \\ V\sin\beta / l_r \\ 0 \end{bmatrix}$$
(29)

Note that the model (29) is written w.r.t. a fixed frame. For a moving sensor frame that does not rotate, model (29) will represent the relative motion of the target vehicle w.r.t. the sensor frame (e.g.,  $\psi$  will be the relative orientation). If the sensor frame rotates, the variables V, A,  $\psi$ , and  $\beta$  no longer represent the true relative speed, acceleration, orientation, and slip angle. But model (29) still will be valid for time-to-collision estimation. The model (29) is in sixth order form but not in the companion form and cannot directly be used for high-gain observer design. Consider the following transformed states and output vectors:

$$z = \begin{bmatrix} X & \dot{X} & \ddot{X} & Y & \dot{Y} & \ddot{Y} \end{bmatrix}^T, y = \begin{bmatrix} X & Y \end{bmatrix}^T \tag{30}$$

The transformed vehicle model can be written as:

We need to calculate f(z) in equation (31):

$$f(z) = \begin{bmatrix} \dot{z}_3 \\ \dot{z}_6 \end{bmatrix} = \begin{bmatrix} \ddot{X} \\ \ddot{Y} \end{bmatrix} = \begin{bmatrix} f_1(z) \\ f_2(z) \end{bmatrix}$$
(32)

The first step is to calculate the acceleration:

$$\ddot{X} = \frac{dV}{dt}\cos(\psi + \beta) - \frac{d(\psi + \beta)}{dt}V\sin(\psi + \beta) \quad (33)$$

$$\ddot{Y} = \frac{dV}{dt}\sin(\psi + \beta) + \frac{d(\psi + \beta)}{dt}V\cos(\psi + \beta)$$
 (34)

Use (29) in (33) and (34):

$$\ddot{X} = z_3 = A\cos(\psi + \beta) - \frac{V^2 \sin \beta}{l_r} \sin(\psi + \beta) \quad (35)$$

$$\ddot{Y} = z_6 = A\sin(\psi + \beta) + \frac{V^2\sin\beta}{l_r}\cos(\psi + \beta) \quad (36)$$

or

$$A\cos(\psi + \beta) = z_3 + \frac{V^2 \sin \beta}{l_r} \sin(\psi + \beta)$$
 (37)

$$A\sin(\psi + \beta) = z_6 - \frac{V^2 \sin \beta}{l_r} \cos(\psi + \beta)$$
 (38)

Rewriting equations (35) and (36) in the following forms:

$$\left(-\frac{V^2 \sin \beta}{l_r} \sin(\psi + \beta)\right) \sin(\psi + \beta)$$

$$= (z_3 - A \cos(\psi + \beta)) \sin(\psi + \beta)$$
(39)

$$\left(\frac{V^2 \sin \beta}{l_r} \cos(\psi + \beta)\right) \cos(\psi + \beta) 
= (z_6 - A \sin(\psi + \beta)) \cos(\psi + \beta)$$
(40)

Subtract (39) from (40):

$$\frac{V^2 \sin \beta}{l_r} = z_6 \cos(\psi + \beta) - z_3 \sin(\psi + \beta) \tag{41}$$

Note that from (29) and (30)

$$\cos(\psi + \beta) = \frac{z_2}{V} \tag{42}$$

$$\sin(\psi + \beta) = \frac{z_5}{V} \tag{43}$$

and velocity is assumed to be non-zero. It is true that vehicles with zero velocity, such as parked cars, will be detected by the RPLIDAR sensor. However, the tracks for such non-moving vehicles will get dropped after recognition that these are non-moving or static objects and are therefore not targets for tracking. This is done in the real-time software which controls how many tracks are updated every sampling interval and which ones do not need to be updated. Using (42) and (43), (41) is written as:

$$\frac{V\sin\beta}{l_r} = \frac{z_6 z_2 - z_3 z_5}{V^2}$$
 (44)

The second step is to calculate jerk from (35) and (36) by considering (28):

$$\ddot{X} = \frac{d(\ddot{X})}{dt} = \frac{dA}{dt}\cos(\psi + \beta)$$

$$-A\sin(\psi + \beta)\frac{d(\psi + \beta)}{dt}$$

$$-2V\frac{dV}{dt}\frac{\sin\beta}{l_r}\sin(\psi + \beta)$$

$$-\frac{V^2\sin\beta}{l_r}(\cos(\psi + \beta))\frac{d(\psi + \beta)}{dt}$$
(45)

$$\ddot{Y} = \frac{d(\ddot{Y})}{dt} = \frac{dA}{dt}\sin(\psi + \beta) + A\cos(\psi + \beta)\frac{d(\psi + \beta)}{dt} + 2V\frac{dV}{dt}\frac{\sin\beta}{l_r}\cos(\psi + \beta) - \frac{V^2\sin\beta}{l_r}(\sin(\psi + \beta))\frac{d(\psi + \beta)}{dt}$$

$$(46)$$

Implementing (27) and (29) in (45) and (46):

$$\ddot{X} = -3A \frac{V \sin \beta}{l_r} \sin(\psi + \beta) - \frac{V^3 \sin^2 \beta}{l_r^2} \cos(\psi + \beta)$$
 (47)

$$\ddot{Y} = 3A \frac{V \sin \beta}{l_r} \cos(\psi + \beta) - \frac{V^3 \sin^2 \beta}{l_r^2} \sin(\psi + \beta) \quad (48)$$

Use (37) and (38) in (47) and (48):

$$\ddot{X} = -3z_6 \frac{V \sin \beta}{l_r} + 2V \left(\frac{V \sin \beta}{l_r}\right)^2 \cos(\psi + \beta) \quad (49)$$

$$\ddot{Y} = 3z_3 \frac{V \sin \beta}{l_r} + 2V \left(\frac{V \sin \beta}{l_r}\right)^2 \sin(\psi + \beta)$$
 (50)

Use (42), (43), and (44) on (49) and (50)

$$\ddot{X} = -3z_6 \frac{z_6 z_2 - z_3 z_5}{V^2} + 2z_2 \left(\frac{z_6 z_2 - z_3 z_5}{V^2}\right)^2$$
 (51)

$$\ddot{Y} = 3z_3 \frac{z_6 z_2 - z_3 z_5}{V^2} + 2z_5 \left(\frac{z_6 z_2 - z_3 z_5}{V^2}\right)^2$$
 (52)

From (42) and (43)

$$V^2 = z_2^2 + z_5^2 \tag{53}$$

Implement (53) on (51) and (52)

$$\ddot{X} = -3z_6 \frac{z_6 z_2 - z_3 z_5}{z_2^2 + z_5^2} + 2z_2 \left(\frac{z_6 z_2 - z_3 z_5}{z_2^2 + z_5^2}\right)^2$$
(54)

$$\ddot{Y} = 3z_3 \frac{z_6 z_2 - z_3 z_5}{z_2^2 + z_5^2} + 2z_5 \left(\frac{z_6 z_2 - z_3 z_5}{z_2^2 + z_5^2}\right)^2$$
 (55)

Summarizing, the transformed model in companion form can be described as follows:

$$\dot{z} = Fz + Gf(z), \qquad y = Hz \tag{56}$$

where

and

$$f(z) = \begin{bmatrix} -3z_6 \frac{z_6 z_2 - z_3 z_5}{z_2^2 + z_5^2} + 2z_2 \left( \frac{z_6 z_2 - z_3 z_5}{z_2^2 + z_5^2} \right)^2 \\ 3z_3 \frac{z_6 z_2 - z_3 z_5}{z_2^2 + z_5^2} + 2z_5 \left( \frac{z_6 z_2 - z_3 z_5}{z_2^2 + z_5^2} \right)^2 \end{bmatrix}$$
(58)

The transformed model in (56) is in companion form and is used for high-gain observer design in the next section. This is the companion form for the multi-output case where the upper diagonal with 1's occurs in block-diagonal-matrix form.

## III. MULTI- OUTPUT HIGH- GAIN OBSERVER DESIGN

While the single output high-gain observer design is well-developed in the literature, the multi-output version is less well-known and is not available in a standard system result format in the literature. In this section, a multi- output high-gain observer is designed for the transformed model (56).

#### A. The Observer Design Formulation

The observer dynamics is:

$$\dot{\hat{z}} = F\hat{z} + Gf(\hat{z}) + L(y - H\hat{z}) \tag{59}$$

Here L is the constant observer gain matrix. The observer error dynamics  $\tilde{z}$  is derived based on (56) and (59):

$$\dot{\tilde{z}} = \dot{z} - \dot{\hat{z}}$$

$$= Fz + Gf(z) - F\hat{z} - Gf(\hat{z}) - L(y - H\hat{z}) \qquad (60)$$

$$= (F - LH)\tilde{z} + G\tilde{f}(z, \hat{z})$$

where  $\tilde{z} = z - \hat{z}$  and  $\tilde{f} = f(z) - f(\hat{z})$ . Here, we assume that the nonlinear process equations are Lipschitz. In other words:

$$\|\tilde{f}_1\|_2 \le \gamma_1 \|\tilde{z}\|_2, \qquad \|\tilde{f}_2\|_2 \le \gamma_2 \|\tilde{z}\|_2$$
 (61)

Define the following transformation for the error variables:

$$e = T^{-1}(\theta)\tilde{z} \tag{62}$$

and

$$T_B(\theta) = \begin{bmatrix} \theta & 0 & 0 \\ 0 & \theta^2 & 0 \\ 0 & 0 & \theta^3 \end{bmatrix}, \qquad T(\theta) = \begin{bmatrix} T_B & 0 \\ 0 & T_B \end{bmatrix}, \qquad \theta > 1$$
(63)

This error conversion definition is the same as that used for the error analysis in the high gain observer for the single output case, but with the revised definition of the matrix  $T(\theta)$  of equation (63). Finding the transformed error variable dynamics by implementing (62) on (60):

$$T(\theta)\dot{e} = (F - LH)Te + G\tilde{f}(z,\hat{z}) \tag{64}$$

or

$$\dot{e} = (T^{-1}FT - KHT)e + T^{-1}G\tilde{f}(z,\hat{z})$$
 (65)

*K* is the transformed observer gain matrix:

$$K = T^{-1}L \tag{66}$$

Note that:

$$T^{-1}FT = \theta F \tag{67}$$

and

$$HT = \theta H \tag{68}$$

Then, (65) is simplified as:

$$\dot{e} = \theta(F - KH)e + T^{-1}G\tilde{f}(z,\hat{z}) \tag{69}$$

**Lemma 1.** There exists  $k_f > 0$  such that:

$$||T^{-1}G\tilde{f}(z,\hat{z})||_{2} \le k_{f}||e||_{2}$$
 (70)

**Proof.** Replacing matrices G and T from (57) and (63):

$$T^{-1}G\tilde{f}(z) = \frac{1}{\theta^3} \begin{bmatrix} 0 & 0 & \tilde{f}_1 & 0 & 0 & \tilde{f}_2 \end{bmatrix}^T$$
 (71)

Using the 2 norm and the Lipschitz bounds of (61):

$$||T^{-1}G\tilde{f}(z,\hat{z})||_{2} = \frac{1}{\theta^{3}} \sqrt{\tilde{f}_{1}^{2} + \tilde{f}_{2}^{2}}$$

$$\leq \frac{1}{\theta^{3}} \sqrt{\gamma_{1}^{2} + \gamma_{2}^{2}} ||\tilde{z}||_{2}$$
(72)

Implement the transformation (62) in (72):

$$||T^{-1}G\tilde{f}(z,\hat{z})||_{2} \leq \frac{1}{\theta^{3}} \sqrt{\gamma_{1}^{2} + \gamma_{2}^{2}} ||Te||_{2}$$

$$\leq \frac{1}{\theta^{3}} \sqrt{\gamma_{1}^{2} + \gamma_{2}^{2}} ||\theta^{3}e||_{2}$$
(73)

The Cauchy-Schwarz inequality gives:

$$||T^{-1}G\tilde{f}(z,\hat{z})||_{2} \leq \frac{1}{\theta^{3}} \sqrt{\gamma_{1}^{2} + \gamma_{2}^{2}} ||\theta^{3}||_{2} ||e||_{2}$$

$$= \sqrt{\gamma_{1}^{2} + \gamma_{2}^{2}} ||e||_{2}$$
(74)

so:

$$k_f = \sqrt{\gamma_1^2 + \gamma_2^2} \tag{75}$$

and the proof is complete.

**Theorem 1.** If there exists P > 0,  $\lambda > 0$ , Q, and  $\theta > 1$  such that:

$$F^T P + PF - H^T Q - Q^T H < -\lambda I \tag{76}$$

and

$$\theta > \theta_0 = \frac{2k_f \lambda_{max}(P)}{\lambda} \tag{77}$$

in which  $\lambda_{max}(.)$  is the maximum eigenvalue, then the estimation error  $\tilde{\mathbf{z}}$  is exponentially stable by taking:

$$K = P^{-1}Q^T \tag{78}$$

**Proof.** Consider the following Lyapunov function candidate:

$$V = e^T P e, \qquad P > 0 \tag{79}$$

and *P* is symmetric. Taking derivative of this Lyapunov function:

$$\dot{V} = \dot{e}^T P e + e^T P \dot{e} \tag{80}$$

and replacing (69) in (80):

$$\dot{V} = \theta e^{T} [(F - KH)^{T} P + P(F - KH)] e + \tilde{f}^{T} (G^{T} T^{-1} P) e + e^{T} (PT^{-1} G) \tilde{f}$$
(81)

Exploiting inner product notation, equation (81) can be

modified as:

$$\dot{V} = \theta e^T [F^T P + PF - H^T K^T P - PKH] e + 2(T^{-1} G \tilde{f}). (Pe)$$
(82)

Using the Cauchy-Schwarz inequality:

$$\dot{V} \le \theta e^{T} [F^{T}P + PF - H^{T}K^{T}P - PKH]e + 2\|T^{-1}G\tilde{f}\|_{2}\|P\|_{2}\|e\|_{2}$$
(83)

For the positive definite Hermitian matrix P:

$$||P||_2 = |\lambda(P)|_{max} = \lambda_{max}(P)$$
(84)

where  $\lambda_i(P)$ , i = 1,2,...,n are the eigenvalues of P, and  $\lambda_{max}(P) = \max_i \lambda_i$  is the largest eigenvalue. Use (70), (78), and (84) in (83):

 $\dot{V} \le e^T [\theta(F^T P + PF - H^T Q - Q^T H) + 2k_f \lambda_{max}(P)I]e$  (85) Based on (76) and (77):

$$\dot{V} \leq e^{T} \left[ -\lambda \theta I + 2k_{f} \lambda_{max}(P) I \right] e 
= \left( -\lambda \theta + 2k_{f} \lambda_{max}(P) \right) e^{T} e < 0$$
(86)

Since V(x) > 0 and  $\dot{V}(x) < 0$ , by the Lyapunov stability criteria, the estimation error converges to zero and so the nonlinear observer is asymptotically stable.

#### B. Synthesis of the Observer Gain for Vehicle Model

In summary, the key steps used in this paper to design the high-gain observer for the vehicle tracking application are:

- Transformation of the system's model into companion form.
- Determination of the Lipschitz constants of the new nonlinear functions in companion form.
- Finding the solution of the observer design LMI to find the observer gain, explained in this section.

In this section, the observer gain L is obtained by solving LMI (76) for  $\lambda = 10$ , using the SEDUMI solver in MATLAB software. We also added the constraint  $P < 30I_{6\times6}$  to limit the  $\lambda_{max}(P)$  and the resulting  $\theta$  from (77). The results are:

$$K = \begin{bmatrix} 11.73 & 20.25 & -7.3 & 0 & 0 & 0 \\ 0 & 0 & 0 & 11.73 & 20.25 & -7.3 \end{bmatrix}^T (87)$$

$$\lambda_{max}(P) = 26.5 \tag{88}$$

Parameter  $k_f$  in (77) depends on the Lipschitz constants of the complex nonlinear functions for this application that are explicitly provided in equation (58). Finding these constants on the  $\mathbb{R}^6$  space is challenging. For simplicity, the constants are calculated for  $\dot{\psi}=c<1$  hyperplanes (constant  $\dot{\psi}$ ). From (29) and (44):

$$\dot{\psi} = \frac{z_6 z_2 - z_3 z_5}{z_2^2 + z_5^2} = c \tag{89}$$

Therefore (58) can be simplified as:

$$f(z) = [-3cz_6 + 2c^2z_2 \quad 3cz_3 + 2c^2z_5]^T \tag{90}$$

The yaw rate c < 1 is in rad/sec and  $3c > 2c^2$ . Hence the Lipschitz constants are 3c and

$$\gamma_1 = \gamma_2 \approx 3c \tag{91}$$

From (75) and (91), 
$$k_f = \sqrt{\gamma_1^2 + \gamma_2^2} = 3\sqrt{2}c$$
. By taking

 $k_f = 1.25$ , we are assuming maximum vehicle Yaw angle rate  $(c_{max})$  of 0.3 rad/s. The observer gain obtained from these assumptions (with  $\theta = 6.7205$ ) is:

$$L = \begin{bmatrix} 67.20 & 823.1 & 2818.5 & 0 & 0 & 0 \\ 0 & 0 & 0 & 67.20 & 823.1 & 2818.5 \end{bmatrix}^{T} (92)$$

Theoretically, any  $\theta > \theta_0$  from equation (77) results in a stable observer. Keeping the value of  $\theta$  minimal helps the observer to perform better in the presence of measurement noise. This is shown in the experimental results, by comparing observer gain (92) with other observer gains obtained using higher values of  $\theta = \{8.6, 8.7\}$ .

#### IV. SIMULATIONS AND EXPERIMENTS

#### A. Simulation Results

In this section, the high-gain observer is compared to a previously designed nonlinear observer based on [13] using MATLAB simulations. The high-gain observer is designed based on a more accurate model compared to the nonlinear observer in [13] which was based on model equation (11) that required the constant velocity assumption. Consequently, it outperforms the other observer (designated as "the LMI nonlinear observer") in most cases, as seen in the simulations.

The three scenarios considered for the simulations are:

- i) the case that the vehicle moves with constant velocity and zero steering angle  $(A = 0, \delta_f = 0)$ ,
- ii) the vehicle moves with constant velocity but with non-zero steering angle  $(A = 0, \delta_f = const)$ , and
- iii) the vehicle moves with constant acceleration and non-zero steering angle  $(A = const, \delta_f = const)$ .

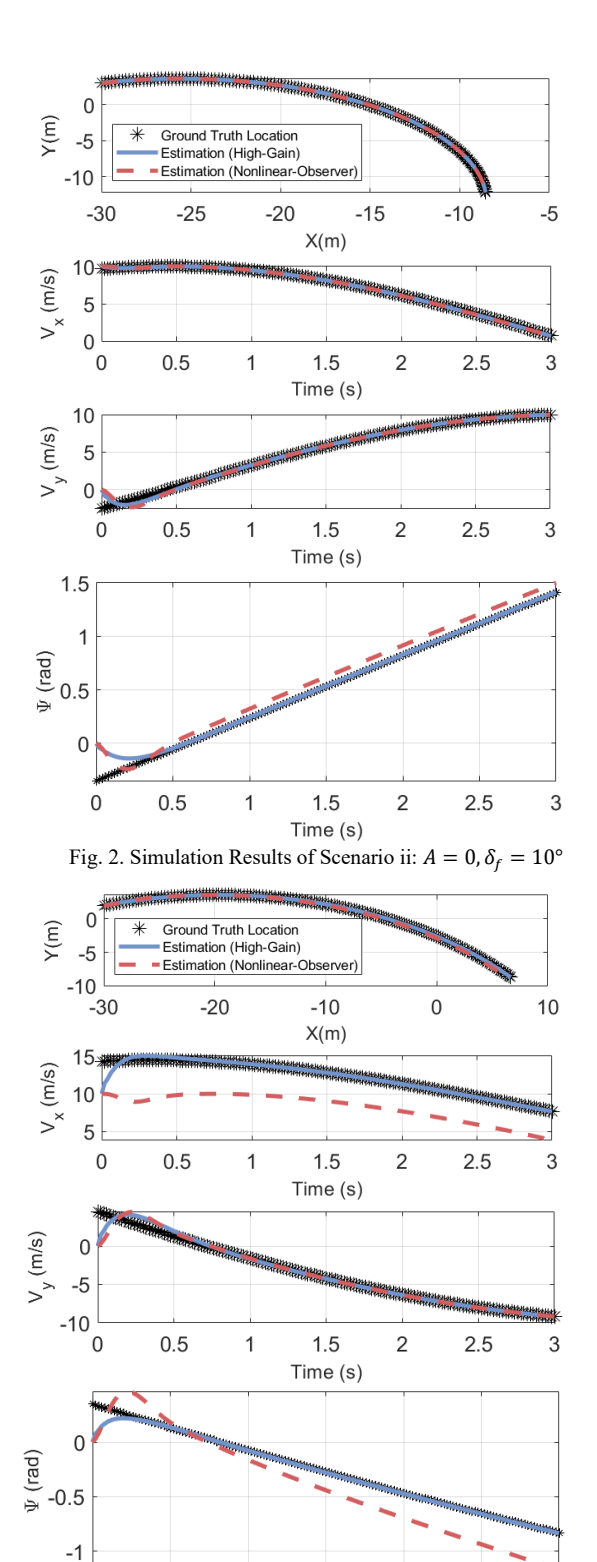
For scenario i), both the high-gain and the LMI nonlinear observers have good performances in tracking the states as acceleration and steering angles are both zero.

Fig. 2 shows the simulation results for scenario ii). Here it can be seen that while the velocities components can still be well estimated, the estimated vehicle orientation angle of the LMI nonlinear observer has a drift compared to the actual vehicle orientation and this drift grows with time.

Fig. 3 shows the simulation results for scenario iii). Here the longitudinal velocity component and the vehicle orientation angle estimated by the LMI nonlinear observer both have significant drift compared to the actual variable values. On the other hand, the high gain observer is able to estimate both variables accurately with no drift.

TABLE I OBSERVERS' RMSE VALUES IN SIMULATIONS

Case #	Observer Type	<i>w</i> (m)	$\widetilde{V_x}$ (m/s)	$\widetilde{V_y}$ (m/s)	$ ilde{\psi}$ (rad)
Simulation 1: $A = 0$ $\dot{\delta} = 0$	Nonlinear	0.01	0.07	0.38	0.04
	High-Gain	0.00	0.05	0.29	0.04
Simulation 2: A = 0 $\dot{\delta} = 10  ^{\circ}/s$	Nonlinear	0.01	0.07	0.4	0.10
	High-Gain	0.00	0.06	0.3	0.05
Simulation 3: $A = -1 \text{ m/s}^2$ $\dot{\delta} = -5 \text{ °/s}$	Nonlinear	0.27	4.09	0.68	0.25
	High-Gain	0.00	0.48	0.55	0.04



Time (s) Fig. 3. Simulation Results of Scenario iii:  $A=-1\frac{m}{c^2}$  ,  $\delta_f=10^\circ$ 

0

0.5

1.5

2

2.5

The root-mean-square errors of the observers for the simulation results are presented in Table 1. The results show that the high-gain observer has the best performance in simulations. The nonlinear observer performs poorly in cases where the speed is variable.

The advantage of the high-gain observer over the LMI-based

nonlinear observer is that the latter assumes a constant velocity, while the former does not make this simplifying assumption and therefore works better in practice. The model theoretically derived for the use of the high gain observer did not involve assumptions on velocity being constant.

## B. EKF vs. High-Gain Observer in Simulation

To illustrate the advantages of the high-gain observer over a standard estimation filter, namely the EKF, we have compared the performance of these estimators for a special scenario shown in Fig. 4. The EKF is designed based on model (29), that includes the acceleration as part of the state vector.

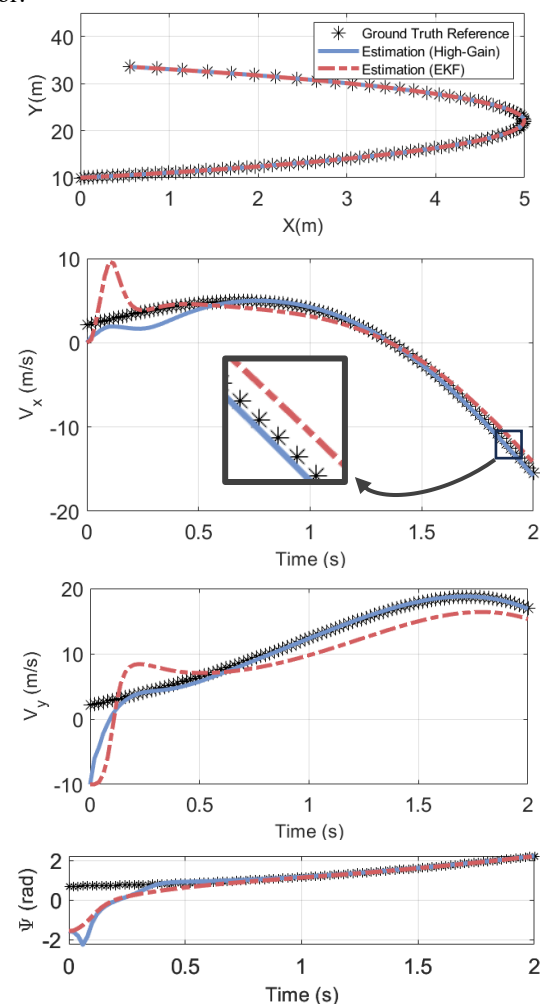


Fig. 4. Simulation Results of Scenario iii:  $A = 10 \frac{m}{c^2}$ ,  $\delta_f = 10^\circ$ 

For both observers, the same initial conditions are used. The initial conditions, however, are taken to be inaccurate and far from the correct state values on purpose, to better compare the convergence properties of the observers. Fig. 4 shows that the high-gain observer works significantly better than the EKF in this case. In the EKF approach, the observer gain varies in each time step, and depends on the state estimate values. Therefore, a wrong initial condition that is far from the true state value might result in a wrong observer gain. The wrong observer gain could cause a low-convergence rate as shown in Fig. 4.

#### C. Experimental Results

In addition to simulations, we performed experiments on tracking vehicle trajectories on a real road traffic intersection using a low-cost (~\$500) RPLIDAR MAPPER sensor mounted on a Ninebot MAX e-scooter. The specifications of this sensor are provided in Table 2. Fig. 5 shows photo of the prototype scooter instrumented with front sensors for tracking vehicles and objects ahead of the scooter. A mounting pole was fabricated and fixed to the scooter so that it is vertical, and sensors mounted on it are aligned with the longitudinal axis of travel. The two sensors mounted on the pole are a monocular camera and the Lidar sensor. The camera is used to record videos for reference. The e-scooter is kept stationary for the experiments. The experimental results presented in this paper consist of real driving scenarios taken from regular vehicles operating on regular roads. Since e-scooters only operate on local low-speed roads and not on highways, the assumptions of low rate of change of acceleration and slip angles for target vehicles are reasonable.

The goal in developing a system on the e-scooter to track vehicle trajectories is to develop a system that can prevent carscooter collisions. By tracking the trajectories of vehicles in the neighborhood of the e-scooter, it is possible to predict whether a particular vehicle poses a danger to the scooter, in which case a loud horn like audio is sounded by the e-scooter to make the car driver aware of the presence of the scooter.

A few samples of the raw readings from the RPLIDAR sensor are shown in Fig. 6. Since the RPLIDAR is a 2D Lidar which continuously rotates 360 degrees while gathering reflected distance data, it only gathers measurements with a frequency of 10 Hz. The raw data of the type shown in Fig. 6 was used for all the estimation results presented in the paper. The data in Fig. 6 shows samples of raw measurements for the case where the target vehicle is moving straight perpendicular to the e-scooter's direction of travel. The right front corner of this vehicle is chosen to be tracked. The estimated trajectory of this vehicle is shown in Fig. 7. Note that the vehicle moves straight from left to right as can be seen in Fig. 6. The orientation estimation in Fig. 7 remains approximately at zero throughout, which agrees with the straight motion along the xaxis. Furthermore, the estimate of longitudinal velocity  $(V_r)$ of the vehicle increases over time, suggesting that the vehicle is accelerating. While the raw data in Fig. 6 does not provide a good idea of the vehicle's trajectory, the estimates from the observer in Fig. 7 clearly provide the lateral and longitudinal positions, velocities and vehicle orientation of the tracked vehicle. We use a forward and backward digital filter (filtfilt) to obtain the reference signals (ground truth) for the states in Fig. 7 and Fig. 8. Note that while future measurements are used to find the reference signals, the high-gain observer only uses the current measurement.

A different experiment is shown in Fig. 8, involving tracking of a vehicle that initially travels on a road perpendicular to the e-scooter's direction and then turns left in front of the e-scooter. The high gain observer provides vehicle trajectory estimates that look very appropriate. The

estimate of the orientation angle for the vehicle goes from 180 degrees to 230 degrees as can be seen in Fig. 8. This result agrees with the left-turning trajectory of the vehicle.



Fig. 5. RPLIDAR sensor and the camera on the Ninebot MAX e-Scooter.

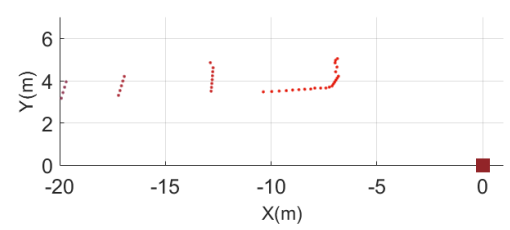


Fig. 6. Samples of the raw data saved in an intersection using the RPLIDAR sensor.

TABLE II RPLIDAR MAPPER SENSOR SPECIFICATIONS

Sensor	Frequency of Data Refresh	Range	Angular Resolution	Accuracy
RPLIDAR MAPPER	10 Hz	0.1-40 m	0.75°	±2 cm

Figs. 9 and 10, compare the experimental results for different values of  $\theta$ . The threshold value of  $\theta = 6.7205$  chosen in section III shows the smoothest performance in the experiments. Higher values lead to significantly more noise in the estimates.

The experiment in Fig. 9 shows the tracking of a vehicle that is travelling in a direction opposite to that of the e-scooter's travel. The vehicle travels straight, coming from a large distance and eventually passing right next to the scooter. This trajectory is nicely estimated, as seen in the y versus x plot at the top of Fig. 9. Further, the estimated velocity components and the vehicle orientation angle are appropriate. The lateral velocity is fairly close to zero while the longitudinal velocity has some variations. The vehicle orientation remains fairly constant at an angle of -90 degrees which agrees with the negative y direction motion of the vehicle. The experiment in Fig. 10 shows a vehicle being tracked which is initially travelling in a direction opposite to that of the e-scooter and then turns left at the intersection just in front of the scooter. Again, the trajectory of the vehicle is well estimated, as seen in the top the y versus x plot of Fig. 10. The orientation of the vehicle changes from roughly -90 degrees to approximately 0 degrees. This agrees with the fact that the vehicle towards the end is travelling in the positive x direction.

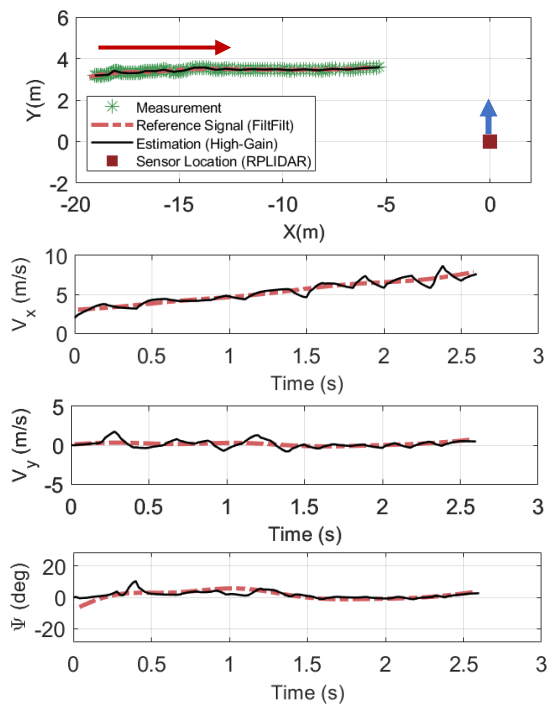


Fig. 7. Estimation results of vehicle 1 which moves straight forward from left to right.

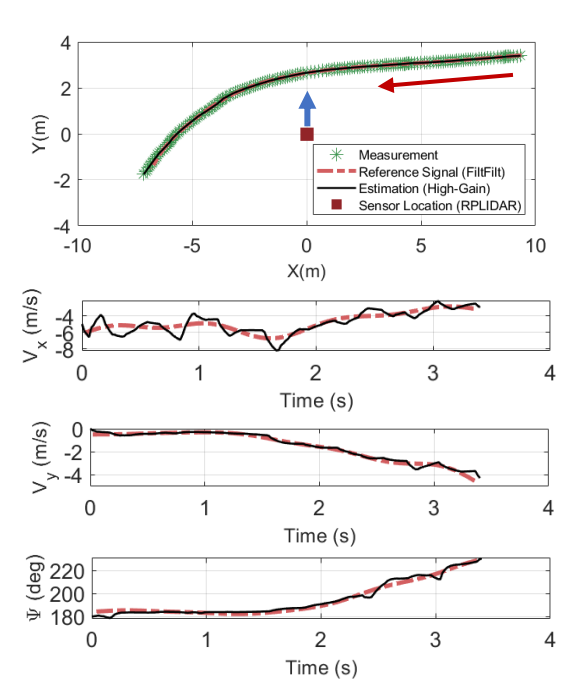


Fig. 8. Estimation results of vehicle 2 which turns left in front of the escooter.

The results of both the simulations and the experiments suggest that the high-gain observer can handle a large range of vehicle orientation angles and can provide stable estimation results with just one constant gain.

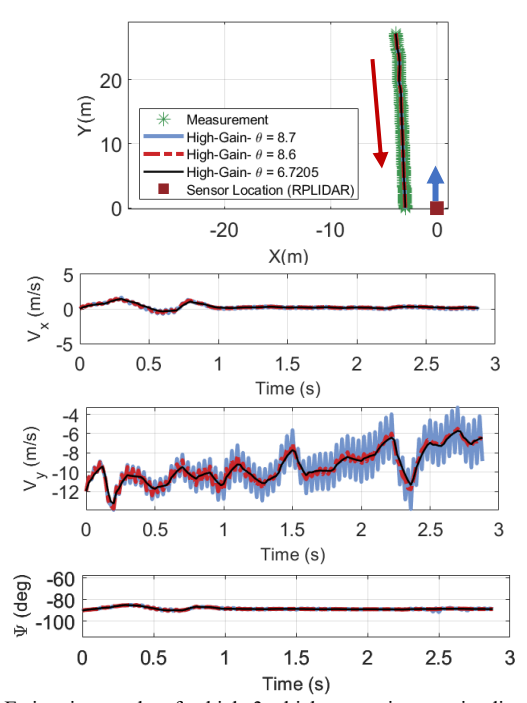


Fig. 9. Estimation results of vehicle 3 which moves in opposite direction to the e-scooter.

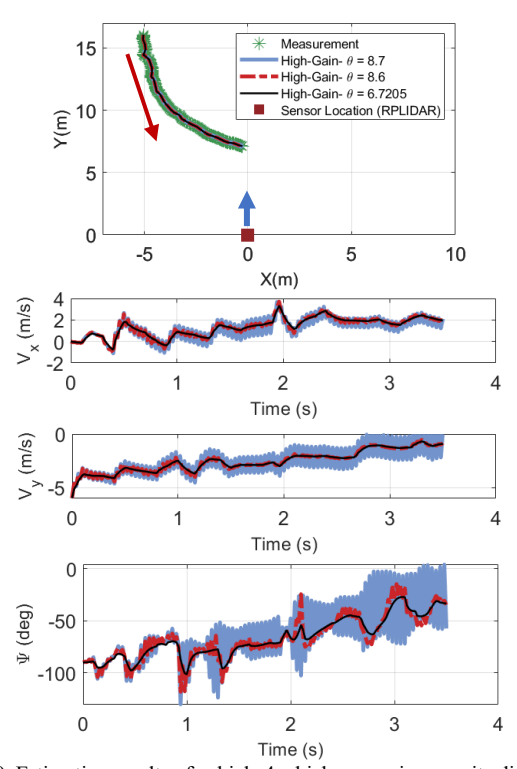


Fig. 10. Estimation results of vehicle 4 which moves in opposite direction and then turns left in front of the e-scooter.

# V. CONCLUSION

In this paper, a multi-output high-gain nonlinear observer was designed for a vehicle trajectory tracking application. The high gain observer approach has the advantages of guaranteed feasibility and stability with one constant observer gain for a wide range of motion. The challenges of transforming the vehicle dynamic model into the companion form needed for

applying the high gain observer technique were addressed. A coordinate transformation that allows for varying velocity and varying slip angle was shown to be appropriate. The high gain observer methodology for a dynamic system with multiple outputs was presented. Finally, simulation and experimental results on vehicle tracking were demonstrated. The experimental results show that, with a high gain observer, vehicle trajectories that span a large range of orientations can be accurately tracked using just one constant observer gain.

#### REFERENCES

- [1] T. Gräber, S. Lupberger, M. Unterreiner and D. Schramm, "A Hybrid Approach to Side-Slip Angle Estimation with Recurrent Neural Networks and Kinematic Vehicle Models," IEEE Transactions on Intelligent Transportation Systems, Vol. 4, No. 1, pp. 39-47, 2019.
- [2] W. Jeon, A. Zemouche, et al, "Tracking of Vehicle Motion on Highways and Urban Roads Using a Nonlinear Observer," *IEEE/ASME Transactions on Mechatronics*, Vol. 24, No. 2, April 2019.
- [3] R. Rajamani, 2011. "Vehicle dynamics and control." Springer Science & Business Media.
- [4] A. Petrovskaya and S. Thrun, "Model Based Vehicle Detection and Tracking for Autonomous Urban Driving," Auton. Robots, vol. 26, no. 2–3, pp. 123–139, Apr. 2009.
- [5] W. Jeon, et al. "A Smart Bicycle That Protects Itself: Active Sensing and Estimation for Car-Bicycle Collision Prevention." IEEE Control Systems Magazine 41.3 (2021): 28-57.
- [6] Y. Bar-Shalom, X. R. Li, and T. Kirubarajan, Estimation with Applications to Tracking and Navigation: Theory Algorithms and Software. Hoboken, NJ, USA: Wiley, 2004.
- [7] Xu, P., Xiong, L., Zeng, D., Deng, Z. et al., "IMM-KF Algorithm for Multitarget Tracking of On-Road Vehicle," SAE Technical Paper 2020-01-0117, 2020, https://doi.org/10.4271/2020-01-0117.
- [8] D. Kim, K. Jo, M. Lee and M. Sunwoo, "L-Shaped Model Switching Based Precise Motion Tracking of Moving Vehicles Using Laser Scanners," *IEEE Transactions on Intelligent Transportation Systems*, Vol. 19, No. 2, Feb 2018.
- [9] K. Jo, M. Lee, J. Kim and M. Sunwoo, "Tracking and Behavior Reasoning of Moving Vehicles Based on Roadway Geometry Constraints," *IEEE Transactions on Intelligent Transportation Systems*, Vol. 18, No. 2, Feb 2017.
- [10] X. Cao, J. Lan, X.R. Li and Y. Liu, "Automotive Radar-Based Vehicle Tracking Using Data-Region Association", *IEEE Transactions on Intelligent Transportation Systems*, Vol. 23, No. 7, July 2022.
- [11] H. Movahedi, A. Zemouche, et al, "Comparative analysis of a nonlinear observer and nonlinear Kalman filters for magnetic position estimation." In 2023 American Control Conference (ACC), pp. 1030-1035. IEEE, 2023.
- [12] Movahedi, Hamidreza, et al. "Hybrid nonlinear observer for battery s tate-of-charge estimation using nonmonotonic force measurements." Advanced Control for Applications: Engineering and Industrial Systems 2.3 (2020): e38.
- [13] R. Rajamani, W. Jeon, H. Movahedi, and A. Zemouche, 2020. "On the need for switched-gain observers for non-monotonic nonlinear systems." in *Automatica*, 114, p.108814.
- [14] A. Zemouche, R. Rajamani, G. Phanomchoeng, B. Boulkroune, H. Rafaralahy, and M. Zasadzinski, 2017. "Circle criterion-based \*\*Mood observer design for Lipschitz and monotonic nonlinear systems—Enhanced LMI conditions and constructive discussions." in \*Automatica\*, 85, pp.412-425.
- [15] H. K. Khalil, 2015. "Nonlinear control" (Vol. 406). New York: Pearson.
- [16] N. Boizot, E. Busvelle, and J. P. Gauthier, 2010. "An adaptive high-gain observer for nonlinear systems." in *Automatica*, 46(9), pp.1483-1488
- [17] A. Zemouche, F. Zhang, F. Mazenc, R. Rajamani, "High-gain nonlinear observer with lower tuning parameter, *IEEE Transactions on Automatic Control*, Vol. 64, No. 8, pp.3194-3209, Nov 20, 2018.



Hamidreza Alai obtained his B.Sc. and M.Sc. degrees in mechanical engineering from the Sharif University of Technology and the University of Tehran, Tehran, Iran in 2016 and 2019, respectively. He is currently pursuing his Ph.D. degree at the University of Minnesota, Twin Cities, MN, USA. His research interests are in

state estimation, control, and mechanism design, including applications in intelligent transportation and robotic systems.



Ali Zemouche received his Ph.D. degree in automatic control in 2007, from the University Louis Pasteur, Strasbourg, France, where he also held a post-doctorate position from October 2007 to August 2008. Dr. Zemouche has been an Associate Professor at the Centre de Recherche en Automatique de Nancy

(CRAN UMR CNRS 7039) at the Université de Lorraine, since September 2008. His research activities include nonlinear systems, state observers, observer-based control, time-delay systems, robust control, learning-based methods, and application to real-world models. Dr. Zemouche is currently associate editor in international journals: SIAM Journal of Control and Optimization, Automatica, IEEE Transactions on Automatic Control, European Journal of Control, and IEEE Systems Journal. He is also a member of the Conference Editorial Board of IEEE Control Systems Society and IFAC TC2.3 (Non-Linear Control Systems).



Rajesh Rajamani (Fellow, IEEE) obtained his M.S. and Ph.D. degrees from the University of California at Berkeley in 1991 and 1993 respectively and his B.Tech degree from the Indian Institute of Technology at Madras in 1989. Dr. Rajamani is currently the Benjamin Y.H. Liu-TSI Endowed

Professor of Mechanical Engineering at the University of Minnesota. His active research interests include sensing and estimation for smart mechanical systems.

Dr. Rajamani has co-authored over 185 journal papers and is a co-inventor on 20 patent applications. He is the author of the popular book "Vehicle Dynamics and Control" published by Springer. Dr. Rajamani has served as Chair of the IEEE Technical Committee on Automotive Control and is currently Senior Editor of the IEEE Transactions on Intelligent Transportation Systems. He is a Fellow of IEEE and ASME and has been a recipient of the CAREER award from the National Science Foundation, the Ralph Teetor Award from SAE, the Charles Stark Draper Award from ASME, the O. Hugo Schuck Award from the American Automatic Control Council, and a number of best paper awards from conferences and journals. Several inventions from his laboratory have been commercialized through start-up ventures co-founded by industry executives. One of these companies, Innotronics, was recently recognized among the 35 Best University Start-Ups of 2016 by the US National Council of Entrepreneurial Tech Transfer.